Nano-Porous Materials for Use in Solar Cells and Fuel Cells

Md Abdullah Al Mamun, Manifa Noor, and Muhammad Hasanuzzaman, Bangladesh University of Engineering and Technology, Dhaka, Bangladesh
Saleem Hashmi, Dublin City University, Dublin 9, Ireland

Introduction

Nano-structured porous silicon (PSi) has become very attractive for solar cell applications as it can be used for anti-reflection coating to absorb more sunlight, omni-directional Bragg reflector to trap the photons by improving internal reflection, and excellent reusable substrate to reduce the cost of wafer. Besides, through deformation, the porosity of porous Si (PSi) allows Ge, GaN and GaAs to grow in an epitaxial way which was nearly impractical for bulk Si and may bring a paradigm shift in next generation thin film photovoltaic research. On the other hand, Dye Sensitized Solar Cell may surpass all other photovoltaic trends not only for its fascinating state-of-the-art fabrication process but also for the prospect of overall cell efficiency, even though the efficiency of DSSC ($\eta \approx 11\%$) is still far behind of PSi ($\eta \approx 18\%$). These porous ceramic solar cells are beneficial especially for low light environment.

Fuel cells are considered as the most efficient and sustainable tool to combat energy crisis and environment pollution because of their higher efficiency in converting chemical energy into electrical energy directly by a combustion and pollution free operation. Fuel cells generate electricity and heat by electrochemical process of redox reaction between fuel (hydrocarbons, H_2) and oxidant (O_2) through porous electrodes, mostly ceramic, and ion conducting non-porous electrolyte. In this paper, the variety of porous ceramic materials for fuel cell application is reviewed briefly.

Porous Ceramics as Solar Cells

Porous Silicon Solar Cell

In 1956, Uhlir and Uhlir first noticed that electrochemical etching creates round shaped pores instead of polishing the Si and Ge wafers which was then quite unusual (Uhlir and Uhlir, 2005). Porous Si wafers have direct and wide bandgap. Si has indirect type 1.12 eV bandgap which means any electromagnetic (EM) spectrum having energy equal or higher than 1.12 eV, it will be absorbed by the material as well as Silicon in this case. This implies that the absorbed EM spectrum definitely have wavelength equal or less than 1107 nm. Consequently the EM spectrum having energy less than 1.12 eV or wavelength higher than 1107 nm will be reflected by the material.

Therefore, Si should be capable of utilizing almost 60%–70% solar spectra but it fails because it enables the Si solar cell to absorb photons having a wide range of energies associated with the spectra. The photoexcitation creates chaotic electron – hole recombination inside of the depletion zone which is undesirable. It is expected that those electrons, generated by photoexcitation, recombine with holes through some specified paths and the travel of electrons through the paths can be utilized. But this expectation hampers when electrons are excited with photons having higher energy than the required bandgap and as a consequence these excess energy turns into heat followed by decreasing the conductivity and ultimately efficiency of the solar cell. In order to increase the efficiency, we need to narrow the solar spectra transmission since we cannot make the solar spectra monochromatic which means we have to increase the bandgap of Si solar cell.

Porous silicon (PSi) as antireflection coating (ARC)

One of the most important factors which limit the efficiency of solar cell is the reflectance of light from its front surface. Due to the refractive index between air and solar cell material, transmission efficiency is highest when incident angle is lowest and with increase in the incident angle, transmission efficiency decreases. From the concept of refractive index which is basically a measure of how much light has been reflected at incident surface, it can be said that to minimize the reflection, the refractive index needs to be decreased. In this way, more light of specific solar spectra (narrowed by increased bandgap) can be transmitted into the solar cell material which in turn increases the net efficiency.

When a thin layer of antireflection coating is placed on the Si solar cell, light is reflected twice – one from the front surface and another from the bottom of the layer. If these two reflected light waves have equal amplitude but out of phase (180°), then they will cancel out each other by resulting a destructive interference (see **Fig. 1(a)**). For the amplitudes of two light waves to be equal, the refractive index of the coating layer has to be equal to the square root of the refractive index of the substrate. Single and multilayer porous silicon structure used as an antireflective coating (ARC) are illustrated in **Fig. 1**.

Although texturizing the front surface has been widely investigated in order to achieve the efficient light trapping, this technique alone could not minimize the reflection below 10% in the wavelength range 400–1000 nm and the reproducibility of state of the art synthesis is another major limiting factor (Dzhafarov *et al.*, 2012; Weiying *et al.*, 2011; Marrero *et al.*, 2009). Hence,

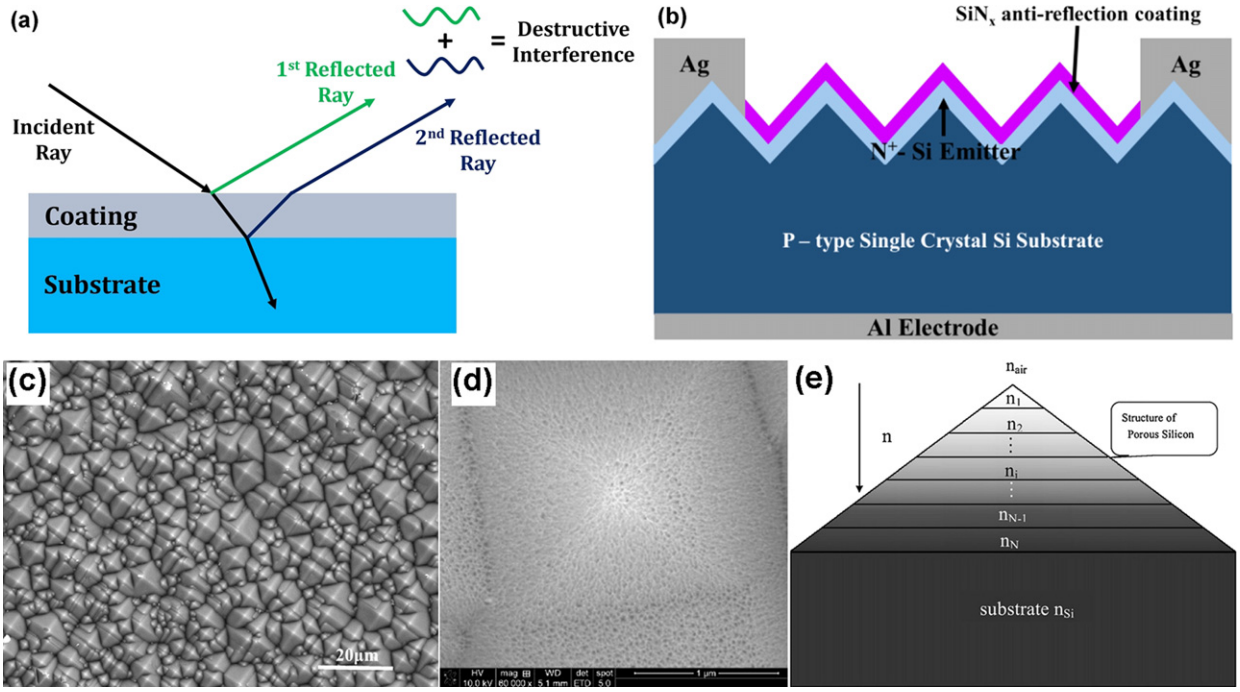

Fig. 1 (a) Schematic diagram of a single layer antireflection coating operation; (b) Schematic diagram of porous Si/textured Si integrated with crystalline Si solar cell; (c) FESEM image of textured Si wafer; (d) FESEM image of one pyramid with porous Si showing uniformity; (e) Schematic multilayer porous Si as ARC, increasing level of darkness and the width of the each film both represent an increasing refractive index (decreasing porosity); $n_{air} < n_1 < n_2 < n_3 < .... < n_N < n_{Si}$. Reproduced from (b) Ho, W.J., *et al.*, 2018. Photovoltaic performance of textured silicon solar cells with MAPbBr3 perovskite nanophosphors to induce luminescent down-shifting, Applied Surface Science 436, pp. 927–933. doi: 10.1016/j.apsusc.2017.12.134. (c)–(e) Lv, H., *et al.*, 2012. Porous-pyramids structured silicon surface with low reflectance over a broad band by electrochemical etching, Applied Surface Science 258 (14), pp. 5451–5454. doi: 10.1016/j.apsusc.2012.02.033.

integration of an antireflection coating has become useful for Silicon solar cell as it reduces the reflectance up to 0.1% and maximizes the efficiency up to 15%–18% (Green *et al.*, 2015; Gao *et al.*, 2018; Kim and Lim, 2015; Silva *et al.*, 2014).

In antireflection coating, the encapsulated and/or front thin layers have refractive index between 1 (air) to 3.84 (bulk Si) which are usually fabricated using plasma enhanced chemical vapor deposition (PECVD) technique. Among them widely investigated Single Layer Antireflection Coatings include SiN_x, Ta_2O_3, ZnS, CeO_2, Al_2O_3 and Double Layer Antireflection Coatings include SiO_2/TiO_2 and ZnS/MgF_2. But it is worth mentioning here that due to state of the art synthesis technique, these ARCs are not cost effective for large scale industrial applications.

While two important pathways – texturizing and vacuum deposited ARCs fade away, integration of porous Silicon as ARC has appeared as a silver lining to reduce the reflection from front surface. Because, the fundamental requirements of antireflection for Single Layer ARC can only be satisfied by one wavelength as well as the light waves reflected from one incident angle and this does not improve much with multilayers introduction on the crystalline Si solar cell. On the other side, refractive index can be easily controlled by varying the porosity in porous silicon (PSi) ARC. Prasad *et al.* (1982) first demonstrated that porous Si as ARC reduces the optical loss from 37% to 8% of silicon solar cell and since then different approaches have been reported by many researchers all around the world. **Table 1** lists such kind of studies which have been reported after 2004.

Porous silicon (PSi) as omnidirectional bragg reflector

Like the optical loss, carrier recombination is equally detrimental for solar energy to current conversion in solar devices. Hence, substitution of metal back reflectors, which are highly absorbing and poor reflector, with dielectric materials offered superior advantages by increasing internal reflection to generate more carriers in active cell. However, due to state of the art deposition techniques, the concept of dielectric materials as omnidirectional Bragg reflector recently has been replaced with a concept of using porous Si for its refractive index tuning compatibility and easier fabrication techniques.

Bhandaru *et al.* (2016) demonstrated that using porous amorphous Si back reflector for amorphous Si solar cell, both short circuit current density and overall cell efficiency were improved by 30% compared to flat metal back reflector amorphous Si solar cell device (For metal back reflector: $\eta = 2.7\%, J_{sc} = 6.5mA/cm^2, V_{oc} = 732mv, FF = 0.57$ and porous amorphous Si reflector: $\eta = 3.5\%, J_{sc} = 8.66mA/cm^2, V_{oc} = 742mv, FF = 0.56$).

Ghannam *et al.* (2010) reported a five layered porous Si back reflectors on back of a textured crystalline Si cell where the bottom two layers had 22.5% porosity (each layer thickness was 157 nm) and the rest three layers had 55% porosity (each layer thickness

Table 1 Porous silicon surface improved antireflection properties with different approaches

Approaches	*Reflectance (%)*	*Wavelength (nm)*	*Ref.*
PSi/textured – Si	4.2	400–900	(Xiao *et al.*, 2010)
PSi/textured – Si	11.34	400–1000	(Chaoui *et al.*, 2013)
PSi/ (n^+ – p) Si	4	400–1000	(Dzhafarov *et al.*, 2012)
PSi/ textured – Si	3.67–6.15	400–1040	(Weiying *et al.*, 2011)
PSi/ textured – Si	<4	400–800	(Marrero *et al.*, 2009)
PSi/ textured – Si	7.5	400–1100	(Druzhinin *et al.*, 2016)
Multilayer PSi/textured – Si	1.9	200–2000	(Lv *et al.*, 2012)
Multilayer PSi/Si (in air)	3	400–1100	(Selj *et al.*, 2011)
Multilayer PSi/Si (under glass)	1.4	400–1100	(Selj *et al.*, 2011)
Multilayer PSi/textured – Si	<5	400–1000	(Kwon *et al.*, 2011)
Double Layer ZnO/PSi/Si	<5	450–850	(Salman *et al.*, 2012)
Double Layer SiO_xN_y/PSi/ polycrystalline Si	<5	500–1000	(Marrero *et al.*, 2009)
Double Layer SiO_2/PSi/Si	3.8	400–1000	(Remache *et al.*, 2010)
Double Layer SiO_xN_y/PSi/ polycrystalline Si	6	450–1100	(Rabha *et al.*, 2011)
Double Layer Al_2O_3/PSi/ monocrystalline Si	7	400–1000	(Rabha *et al.*, 2013)
Double Layer SiO_xN_y/PSi/Si	0.01	430–670	(Search *et al.*, 2006)
Double Layer SiO_xN_y/PSi/Si	<7	400–900	(Search *et al.*, 2006)
Double Layer DLC/PSi/Si	<2.5	400–850	(Aroutiounian *et al.*, 2004)
Double Layer DLC/PSi/Si	≈ 1	400 and 700 nm only	(Aroutiounian *et al.*, 2004)

was 256 nm). The overall cell efficiency (η), short circuit current density (J_{sc}), open circuit voltage (V_{oc}) and fill factor (FF) were found as 12%, 26.99 mA/cm^2, 609.2 mv and 0.73 respectively.

Kuzma-Filipek *et al.* (2008) showed that low (23%)/high (42%)/low (23%)/…./high (42%) porosity Si layers as back reflector on crystalline Si exhibits internal reflection R_B of 95% in 900–1050 nm wavelength region for 20 bilayers and in 800–1100 nm wavelength region for 60 bilayers. The overall cell efficiency (η), short circuit current density (J_{sc}), open circuit voltage (V_{oc}) and fill factor (FF) for 40 bilayers and 60 chirped bilayers were found as 13.3%, 28.7 mA/cm^2, 598 mv, 0.78 and 13.9%, 29.6 mA/cm^2, 605 mv, 0.78 respectively.

Bougoffa *et al.* (2017) investigated the improvement of internal reflection by stacking multiple layers of porous Si as back reflectors on textured crystalline Si solar cell. They showed that for single double–porosity Si layer, internal reflection R_B increases from 18% to 40% due to porosity variation. Again, for three double–porosity Si layers, the porosity variation improved internal reflection R_B from 51% to 80% as depicted in **Fig. 2**.

Multiple bilayer porous Si back reflectors, improved the internal reflection, have been reported in several literatures i.e., R_B = 62% for multicrystalline Si and more than 90% for single crystalline Si (Ivanov *et al.*, 2013), R_B = almost 100% except for a small dip for p polarized light which can be minimized by chirped like approach and bilayer comprised 70% and 20% porosity Si (Jiang *et al.*, 2014), R_B = 80% for 15 bilayer low and high porosity Si (Kuzma-Filipek *et al.*, 2007), R_B = 86% for single layer Si/PSi comprising 60% porosity and R_B = 83% for Si/PSi/SiN_x (Remache *et al.*, 2016).

Porous silicon (PSi) as a promising substrate for thin film solar cell

Layer transfer process using porous silicon as reusable substrate has raised enormous enthusiasm among researchers since last decade for its promising cost effectiveness and facile state of the art fabrication techniques. In a typical layer transfer process to make thin crystalline Si solar cell as depicted in **Fig. 3**, a monocrystalline silicon wafer is first electrochemically etched which turns it into a porous Si wafer comprised of two different porosity layers – low (20%–30%) and high (above 50%). Appropriate annealing allows the low porosity layer to act as an excellent monocrystalline ground for growing epitaxial Si on it. Once the epitaxial layer is deposited, the epitaxial layer with low porosity Si layer can be detached through the high porosity layer and thus the remaining high porosity Si wafer becomes further reusable. However, the process sequence i.e., detachment of epitaxial Si layer from high porosity Si substrate, gluing that on a foreign substrate and device fabrication on epitaxial Si layer may vary depending on the research requirements (Solanki *et al.*, 2004).

Brendel *et al.* (2003) achieved 15.4% cell efficiency for 25 μm thick crystalline Si solar cell where short circuit current density (J_{sc}), open circuit voltage (V_{oc}) and fill factor (FF) were found as 32.7 mA/cm^2, 623 mv and 0.755, respectively. Later, Reuter *et al.* (2009) fabricated 50 μm thick crystalline Si solar cell of 17% cell efficiency where short circuit current density (J_{sc}), open circuit voltage (V_{oc}) and fill factor (FF) were found as 36 mA/cm^2, 634 mv and 0.746 respectively. Petermann *et al.* (2012) improved the cell efficiency to 19.1% for a 43 μm thick crystalline Si solar cell where short circuit current density (J_{sc}), open circuit voltage (V_{oc}) and fill factor (FF) were found as 37.8 mA/cm^2, 650 mv and 0.776, respectively. Wang *et al.* (2014) used steel as foreign substrate and achieved 16.8% cell efficiency for 18 μm thin Si solar cell with short circuit current density (J_{sc}), open circuit voltage (V_{oc}) and fill factor (FF) were found as 34.5 mA/cm^2, 632 mv and 0.77, respectively.

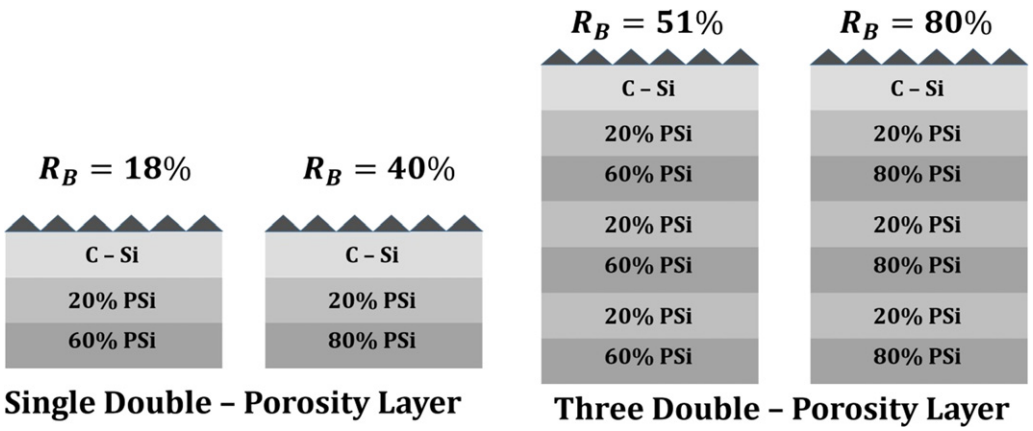

Fig. 2 Multiple stacking of porous Si layers enhanced internal reflection. Reproduced from Bougoffa, A., *et al.*, 2017. Analytical model of front texturization effect on silicon solar cell with porous silicon at the backside, Optical and Quantum Electronics 49 (1), pp. 1–13. doi: 10.1007/s11082-016-0864-8.

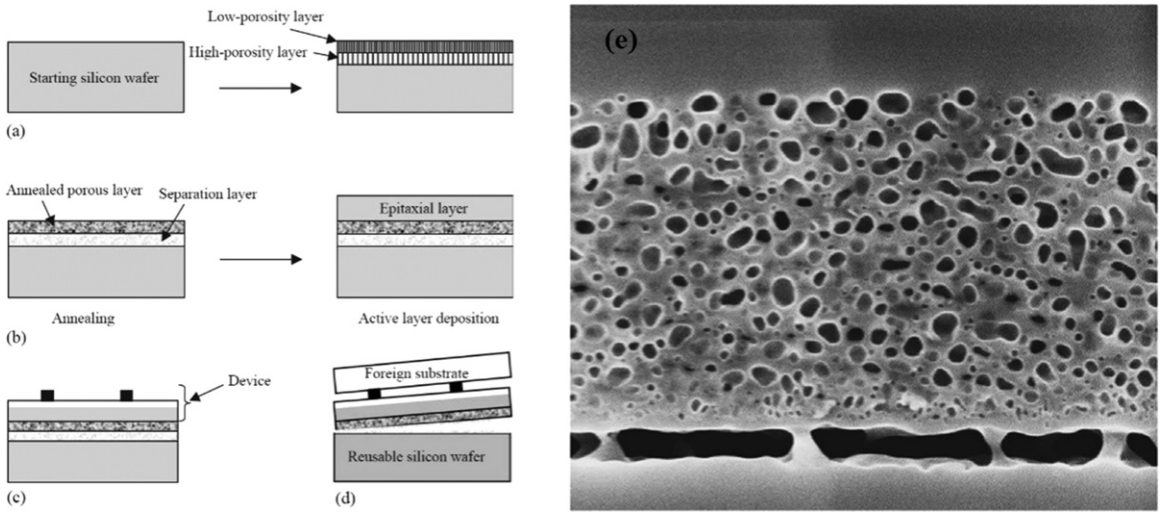

Fig. 3 Steps of porous layer transfer processes using porous silicon as a sacrificial layer for obtaining thin monocrystalline silicon films on cost-effective substrates: (a) a double porosity structure (high-porosity layer beneath low-porosity layer) formation on starting silicon substrate by anodization; (b) thermal annealing of porous silicon and active layer deposition: annealed low-porosity layer acts as a good seeding layer for epitaxial layer deposition and voids with weak silicon pillars form in high-porosity layer acts as a separation layer; (c) Device fabrication; (d) Separation of epitaxial layer from the starting silicon substrate and transfer onto foreign substrate by gluing it with an adhesive layer and applying mechanical force; (e) SEM image showing epitaxial layer/low porosity/high porosity/Si wafer. Reproduced from (a)–(d) Solanki, C.S., *et al.*, 2004. Porous silicon layer transfer processes for solar cells, Solar Energy Materials and Solar Cells 83 (1), pp. 101–113. doi: 10.1016/j.solmat.2004.02.016. (e) Radhakrishnan, H., *et al.*, 2015. Kerfless layer-transfer of thin epitaxial silicon foils using novel multiple layer porous silicon stacks with near 100% detachment yield and large minority carrier diffusion lengths, Solar Energy Materials and Solar Cells 135, pp. 113–123. doi: 10.1016/j.solmat.2014.10.049.

Apart from thin film Si solar cell, porous Si has appeared as a remarkable buffer layer for Ge (Calabrese *et al.*, 2014; Aouassa *et al.*, 2012; Mahamdi *et al.*, 2018; Gouder *et al.*, 2014), GaN (Abud *et al.*, 2016; Wu *et al.*, 2018) and GaAs (Wilkins *et al.*, 2013) epitaxial growth. The compatibility of porosity variation allows PSi to deform during epitaxial growth which is not possible for bulk Si due to its large lattice mismatch with those materials and thus porous Si resembles as a promising substrate for multi-junction solar cell devices.

Dye Sensitized Solar Cell

A dye sensitized solar cell is comprised of four different components: photoanode, dye sensitizer, electrolyte and electrode. Usually porous TiO_2 is used as photoanode which is covered by a thin layer of dye sensitize materials. When sunlight strikes the surface of the thin layer, dye sensitizers get excited and they pass the photon excited electrons to the TiO_2 film which later travelled through

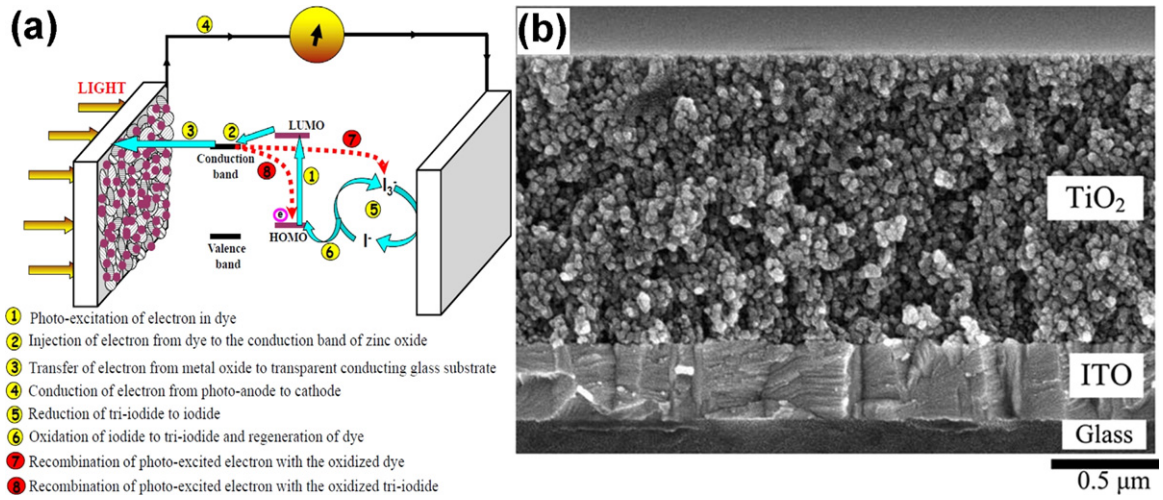

Fig. 4 (a) Schematic working principle of Dye Sensitized Solar Cell (DSSC); LUMO means Lowest Unoccupied Molecular Orbitals and HOMO means Highest Occupied Molecular Orbitals; (b) A cross-sectional photograph of TiO_2 thin film with a film thickness of 1.5 μm. Reproduced from (a) Sengupta, D., *et al.*, 2016. Effects of doping, morphology and film-thickness of photo-anode materials for dye sensitized solar cell application – A review, Renewable and Sustainable Energy Reviews 60, pp. 356–376. doi: 10.1016/j.rser.2016.01.104. (b) Kao, M.C., *et al.*, 2009. The effects of the thickness of TiO_2 films on the performance of dye-sensitized solar cells, Thin Solid Films 517 (17), pp. 5096–5099. doi: 10.1016/j.tsf.2009.03.102.

the electrolyte. The redox coupled electrolyte (typically $I_3^- and I^-$) is attached with a counter electrode to collect the electrons and regenerate the dye. The overall efficiency (η) of DSCC is measured by the following equation:

$$\eta = \frac{V_{oc} J_{sc} FF}{P_{in}} \tag{1}$$

Where, V_{oc} is the open circuit voltage which is actually the measure of the potential difference between TiO_2 and redox potential of electrolyte; J_{sc} is the short circuit current which depends on the light harvesting efficiency of dye sensitizers, electronic conductivity performance of electrolyte and charge collection efficiency of counter electrode; FF (fill factor) represents the ratio of maximum generated power to the product of open circuit voltage and P_{in} is the power of incident light (standard irradiation condition: 100 $mW/cm^2, AM1.5$). Working principle of Dye Sensitized Solar Cell (DSSC) is depicted in **Fig. 4**.

A review on photovoltaic parameters of Dye Sensitized Solar Cell (DSSC) using different approach and photoanode is listed in **Table 2**.

Porous Ceramics as Fuel Cells

Energy crisis and environmental pollution are the most alarming issues of today's world. Burning of fossil fuels to meet energy requirement have not only reduced the finite reserves of but also caused greenhouse effect by releasing harmful gases. The quest for efficient utilization of renewable energy (like solar, wind energy etc.) and development of sustainable, green energy sources have gathered enormous interest among the researchers. Fuel cells provide a key solution to conversion and storage of energy. In 1838 William Grove invented the first fuel cell by reversing electrolysis of water and named it "wet cell battery" or "Grove cell" (Grove, 1839). Various fuel cells have been developed since then based on electrode and electrolyte types that are listed in **Table 3**.

Among the varieties of fuel cells, Solid Oxide Fuel Cells (SOFC) and Polymer Electrolyte Membrane (PEM), also known as proton-exchange membrane fuel cell, are most commonly used. In PEM fuel cells, electrolyte material is polymer based, generally PTFE/Teflon and solid (Ni, Ti, stainless steel mesh, porous Carbon) materials are used as electrodes and Pt coated as catalyst on the anode. Each type of fuel cells has its own advantages and limitations. As it can be seen from **Table 3** that most of the fuel cells use hydrogen as their fuel which is more costly to produce than other source of energy and it is almost energy neutral (required production energy roughly equal to as it delivers at the end destination). Therefore, the applications of fuel cells are so far very limited. Solid Oxide Fuel Cells (SOFC) has received renewed attention because of hydrogen extraction process. A high operating temperature here allows hydrogen to be extracted directly from natural gas through a catalytic reforming process. Due to the renewed research interest and future prospect, we limit our discussion to SOFC in this paper.

Solid Oxide Fuel Cell

Gaugain first discovered solid electrolyte in 1853 and in 1899 Nernst showed that the conductivity of Y_2O_3 doped ZrO_2 (15 YSZ) rises with increasing temperature (Gaugain, 1853; Nernst, 1899). Baur and Preis finally developed SOFC in 1937

Table 2 Photovoltaic parameters of DSSC using different approach and photoanode

Photoanode	*η (%)*	*V_{oc} (mV)*	*J_{sc} (mW/cm^2)*	*FF (%)*	*Ref.*
TiO_2 nanosphere	8.5	730	17.88	65	(Ye *et al.*, 2013a)
TiO_2 microsphere	7.94	690	15.42	66	(Wang *et al.*, 2013a)
TiO_2 nanosphere	11.18	846	17.73	75	(Humphry-Baker *et al.*, 2013)
TiO_2 nanorod	4.4	739	8.88	67	(Hafez *et al.*, 2010)
TiO_2 nanorod	7.91	700	20.49	54.5	(Lv *et al.*, 2013)
TiO_2 nanofiber	4.01	770	8.67	60	(Song *et al.*, 2004)
TiO_2 nanosphere	8.44	804	14.57	51.9	(Ye *et al.*, 2013b)
TiO_2 nanofiber	10.30	640	22.4	72	(Chuangchote *et al.*, 2008)
TiO_2 nanofiber	10.20	795	17.48	73.3	(Mukherjee *et al.*, 2009)
TiO_2 nanowire	9.95	792	16.22	77.5	(Wang and Bai, 2014)
TiO_2 nanorods	9.21	750	17.75	70	(Kathirvel *et al.*, 2016)
Cr doped TiO_2	8.4	780	15.2	71	(Kim *et al.*, 2008)
Sn doped TiO_2	8.31	722	16.01	70.7	(Duan *et al.*, 2012)
W doped TiO_2	9.1	610	19.31	77	(Zhang *et al.*, 2015)
TiO_2/Au@GO NPs	9.06	780	17.19	67.6	(Kwon *et al.*, 2016)
Al_2O_3 – TiO_2 nanospheres	8.60	730	16.9	70	(Wang and Bai, 2014)
$TiCl_4$ treated TiO_2 nanospheres	10.52	776	19.62	69.1	(Ye *et al.*, 2013b)
TiO_2 nanorod/ TiO_2 nanosphere	10.34	827	18.78	67	(Yan *et al.*, 2011)
TiO_2 nanorod/ TiO_2 nanosphere	7.1	756	14.45	65	(Hafez *et al.*, 2010)
ZnO nanowire/TiO_2 nanosphere	8.44	763	16.08	68.8	(Yang *et al.*, 2017)
TiO_2/ZnO nanodonuts	9.0	780	16.70	69	(Li *et al.*, 2015)

Table 3 Types of fuel cells

	Polymer Electrolyte Membrane (PEM)	*Alkaline Fuel Cell (AFC)*	*Phosphoric Acid Fuel Cell (PAFC)*	*Molten Carbonate Fuel cell (MCFC)*	*Solid Oxide Fuel Cell (SOFC)*
Fuel	H_2	H_2	H_2, external reformate	H_2, CO, CH_4	H_2, CO, CH_4
Common Anode	Ni/Pt	Pt	Pt	Ni alloy	Ni/YSZ cermet
Common Cathode	Ni	Pt	Pt	NiO	$LaMnO_3$ (LSM)
Common Electrolyte	Perflurosulfonic acid	KOH (aq)	Phosphoric acid	Molten Li/Na/K carbonates	Yttria Stabilized Zirconia (YSZ)
Operating Temperature	<120°C	<100°C	150–200°C	600–700°C	500–1000°C
Electrical Efficiency	60% (direct H_2) 40% (reformed fuel)	60%	40%	50%	60%

having an operating temperature 1000°C (Baur and Preis, 1937). Most of the SOFCs operate at very high temperature of 800–1000°C, which causes material degradation and, as a result, incur higher maintenance cost. Therefore, researchers, especially in last two decades, focused on developing intermediate (500–800°C) range SOFCs (Mahato *et al.*, 2015; da Silva and de Souza, 2017). The main advantages of SOFC are the lower cost compared to solar and wind energy, less greenhouse gas emission, durability, noise-free power generation, direct conversion of chemical energy to electrical energy and reliability. During 2004–2006 alone, the cost of fuel cell unit reduced from $8000/KW to $4800/KW (Shaikh *et al.*, 2015; Shahid Rafique *et al.*, 2018). However, more attention in research is now given to further reduce the unit cost of SOFC by developing new and efficient electrode materials.

Starting from Ni-cermet anodes and LSM ($LnSrMnO_3$) cathodes, a wide range of ceramic materials has been explored for enhancing the efficiency and lowering the working temperature of Solid Oxide Fuel Cells. Porosity and its characteristics play a major role for efficiency enhancement of SOFC. When porosity is >25%, gas phase becomes fully in contact with the Triple Phase Boundary (TPB). For effective performance, optimum porosity of the electrodes are estimated to be 36%–48% (Bertei and Nicolella, 2011; Yang *et al.*, 2015). Pore size and distribution are also controlling factors of gas flow inside the electrodes.

Working Principle of SOFC

The main components of SOFC are porous electrodes (anode and cathode) and solid electrolyte that is sandwiched between the two electrodes. Both electrodes and electrolyte are ceramic material. Porous anode and cathode are electronic conductors and the

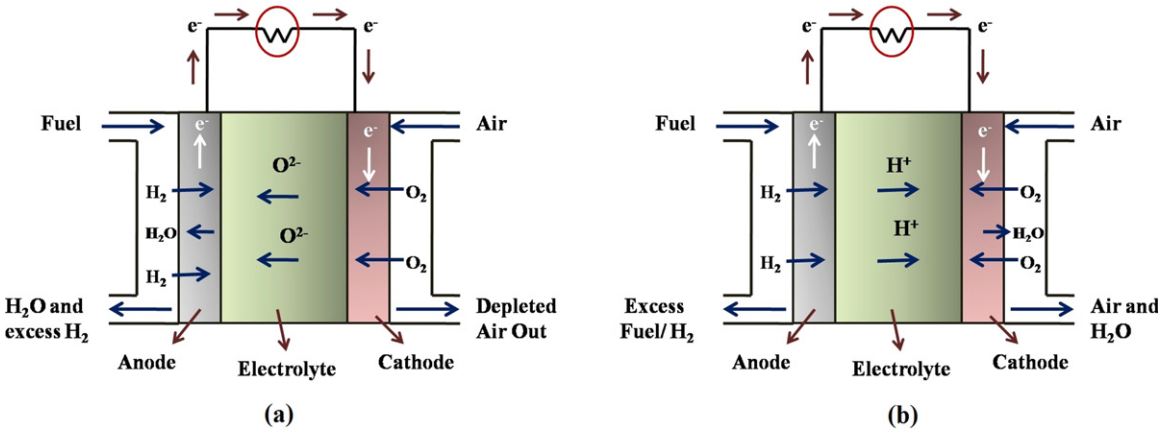

Fig. 5 Schematic diagram of SOFC working principle having (a) oxide ion conducting electrolyte, and (b) proton conducting electrolyte.

Table 4 Evolution of nanoporous anode materials

Material	*Processing method*	*Porosity*	*Operating temperature (°C)*	*Electrolyte/Cathode*	*Maximum power density (mW/cm²)*	*Ref.*
Ni-YSZ Cermet (50% Ni-50% YSZ)	Tape casting, fired at 950°C	20%–40%	1000	8YSZ/ LSM-8YSZ	1900	(Dees *et al.*, 1987; Ivers-Tiffee *et al.*, 1990; Lee *et al.*, 2002)
Ni-SDC (50%–60% Ni)	Uniaxial pressing, 1200°C	5%–10%	800	YSZ/LSM-YSZ	980	(Chen *et al.*, 2008b; Mantzouris *et al.*, 2008)
NiOScSZ-10Sc-1Ce-SZ	Microtubular design	37%	600	ScCeSZ/ LSCF-GDC	200	(Suzuki *et al.*, 2009)
NiO (nanoporous)	Impregnation, calcination 700°C	Pore dia 40nm	650 550	LSGM/LSCF-LSGM	1200 390	(Zhan *et al.*, 2011)
Ni-CeO_2Ni-Sm_2O_3Ni-Eu_2O_3Ni-Gd_2O_3	Uniform pressing	~32%–45%	600	$Gd_{0.1}Ce_{0.9}$ $O_{1.95}$ /$Sm_{0.5}Sr_{0.5}CoO_3$	600	(He *et al.*, 2010)
NiO-$Gd_{0.1}Ce_{0.9}$ $O_{1.95}$	Tape casting, spray coating	~28%	650 600 550 500	GDC/LSCF-GDC	909 623 335 168	(Fu *et al.*, 2010)
Ag-CGO (Ag 45%)	Pressing, sintering 1500°C	48%	650	CGO ($Ce_{0.8}Gd_{0.2}O_{1.9}$)/ LSCF	790	(Wang *et al.*, 2008)
Pd (nonporous)	DC Sputtering	Pore gap 8 nm	400	YBaZrO3-Pt	72.4 (H2) 15.3 (ethanol)	(Li *et al.*, 2017)
Perovskite Anodes						
La doped STO ($La_{0.2}Sr_{0.7}TiO_3$)	Solid state, Sintering 1450°C	40%–60%	750	LSC-YSZ	500	(Savaniu and Irvine, 2011)
$Li_{0.33}La_{0.56}TiO_3$ (LLTO) coated SmCeO (SDC)	Solution infiltration, firing 900°C	50%	800	SDC/SDC-BSCF	123–215	(Wang *et al.*, 2015)
$Sm_{0.5}Ba_{0.5}MgO_{3-\delta}$ (SBMO)	Pechini method, Calcination 950°C	High porosity	850	LSGM (LaSrGaMgO)/ BSCF (BaSrCoFeO)	150 (H_2) 415 (methanol)	(Zhao *et al.*, 2017)

electrolyte is dense, impervious and ion/proton conductor. Anode and cathode are externally connected. The anode side (also called Fuel side) receives H_2, hydrocarbons or methanol as a fuel, oxidizes them and generates electrons that flow through external circuit. Oxygen (or oxidant) is reduced at the triple phase boundary of cathode, gas and electrolyte. Generated oxide ions diffuse through ion conducting electrolyte via vacancy hopping mechanism at high temperature (800–1000°C). High temperature enables and makes the electrolyte ion conductor. At the anode-electrolyte-gas triple phase boundary (TPB), H_2 and O_2- ions react to form H_2O (Mahato *et al.*, 2015; Shaikh *et al.*, 2015; Kee *et al.*, 2008). A schematic diagram of SOFCs operating principle is presented in **Fig. 5**.

Table 5 Evolution of nanoporous cathode materials

Material	*Processing method*	*Porosity*	*Operating Temperature (°C)*	*Maximum Power Density (mW/cm²)*	*Ref.*
$Sm_{0.2}Ce_{0.8}O_{1.9}$ (SDC) and $Sm_{0.5}Sr_{0.5}CoO_3$ (SSC)	Spin coating	Small, inter-connected pores	600	300	(Chen *et al.*, 2011)
LSM ($La_{0.8}Sr_{0.2}MnO_{3-\delta}$) cathode supporter and LSM–$Sm_{0.2}Ce_{0.8}O_{2-\delta}$ (SDC) cathode functional layer (CFL)	Slurry spin coating	23%–33%	850	580	(Chen *et al.*, 2012)
$Ba_{0.5}$ $Sr_{0.5}$ $Co_{0.8}$ $Fe_{0.2}$ $O_{3-\delta}$(BSCF)	Spray coating	Highly porous cathode, homo-geneous pores	800 600	432 145	(Shi *et al.*, 2012)
YSZ-$Mn_{1.5}$ $Co_{1.5}$ O_4 (MCO) composite	Pressing 3000 PSi, sintering 1450°C	55%	800	0.15 Ωcm² (lowest polarization resistance)	(Zhan *et al.*, 2013)
$(La_{0.8}Sr_{0.2})_{0.95}MnO_3$ (LSM95)	Tape casting	33.76%–45.50%	750	325	(Wang *et al.*, 2013b)
$La_{0.6}$ $Sr_{0.4}$ $Co_{0.2}$ $Fe_{0.8}$ O_3 and Gd-doped ceria (LSCF-GDC)	Screen printing, sintering 1200°C	Highly porous	750	0.38–0.83 Ωcm² (polarization resistance)	(Liu *et al.*, 2013)
Double perovskite $SmBaCo_{2-x}Ni_xO_{5+\delta}$ ($SBCN_x$) ($x = 0$–0.5)	Screen printing	Porous cathode	800	536	(Xia *et al.*, 2016)
$Sm_{0.5}Sr_{0.5}CoO_{3-\delta}$ (SSC)	Electro spinning	Very porous nano fiber cathode	700	1090	(Chang *et al.*, 2015)
$NdBaFe_{2-x}Mn_xO_{5+\delta}$ ($0.0 \leq x \leq 0.3$)	Citric acid- nitrate process, sintering 1200°C	Porous cathode	500–700	453	(Mao *et al.*, 2015)
$Sr_xCo_{0.7}Nb_{0.1}Fe_{0.2}O_{3-\delta}$ (SCNF, $x = 0.95$ and 1)	Screen printing	Moderate porosity	700	208–180	(Ding *et al.*, 2017)

Materials Used in SOFC

Anode

Anode is the most important component of SOFC where the oxidation of fuel takes place. An anode must possess enough porosity, electrical conductivity and chemical compatibility with electrolyte at operating temperature. The following reaction takes place at anode-

$$H_2 + O^{2-} \rightarrow H_2O + 2e^-$$

Electro-catalytically active and high electronic conductivity makes cermet based anodes, e.g., Ni-YSZ (8 mol% Y_2O_3 and ZrO_2), most commonly used anode material. However, some limitations associated with Ni-YSZ anode at the SOFC operating temperature are Ni sintering, deposition of Carbon (from hydrocarbon fuels) and Sulfur poisoning. To overcome these drawbacks of Ni based cermets, many studies have been conducted for increasing the stability, durability and electrical conductivity of anodes like: Ni-YSZ anodes modified with Ag (Wu *et al.*, 2016), Al_2O_3 (Song *et al.*, 2016); Ni-SDC (Chen *et al.*, 2008a), Ni-GDC (Fu *et al.*, 2010), Ce based cermets ($Ce_xZr_{1-x}O_2$) (Kearney and Baker, 2012), LnSTMperovskites (Ln=La, Nd, Sm) (Jeong *et al.*, 2015), $PbMO_3$ ($Pr_{0.5}Ba_{0.5}MnO_{3-\delta}$) (Sun *et al.*, 2016) etc. Double perovskite based materials have been reported as well and claimed to be exhibited longer life and highest efficiencies. Various anode materials along with their efficiency and porosity are listed in **Table 4**.

The efficient anode must contain the following chief characteristics:

- High electrical conductivity at operating temperature
- Sufficient electrochemical and catalytic activity for the oxidation.
- Minimal CTE mismatch with other adjacent cell components
- Fuel flexible and able to tolerate carbon deposition and sulfur poisoning.
- Chemical and thermal stability.
- Sufficient mechanical strength to withstand mechanical stress at high operating temperature.
- High porosity (20%–40%) for smooth fuel migration and the reaction product release (Singhal, 2000).

Cathode

Cathode is a porous electrode where reduction of O_2 takes place. Materials selection for cathode should be such that it possesses high electronic conductivity, stability and it remains unreactive to electrolyte materials at high operating temperature. In cathode, the following reaction takes place:

$$\frac{1}{2}O_{2(gas)} + 2e^- \rightarrow O^{2-}$$

$Ln_{1-x}Sr_xMnO_3$ (LSM perovskite) is used as most common cathode material (Chen *et al.*, 2012). Researches have been conducted on LSM/GDC cathodes (Ahmed *et al.*, 2014), $LnBaCoO_{5+\delta}$ (Ln= La, Pr, Nd, Sm, Gd, Y) (Xia *et al.*, 2016) and NBCO ($NdBaCu_2O_{5+\delta}$) (Kong *et al.*, 2015) cathodes along with $A_2BO_{4+\delta}$ (A= rare- earth material, B=Cu, Fe, Ni) based composite cathodes (Ferkhi and Ahmed, 2016; Kolchugin *et al.*, 2016). Dependence of Maximum Power Density of SOFC on cathode material and porosity is presented in **Table 5**.

For an efficient operation of SOFC, the cathode should possess the following functionalities:

- High electronic conductivity (preferably more than 100 S/cm in an oxidizing atmosphere)
- Minimal or no CTE mismatch with other components of the cell
- Chemical compatibility with electrolyte and interconnect materials
- Porous structure to allow fast diffusion of O_2 from cathode to cathode-electrolyte interface
- High ionic conductivity
- Good oxidizing stability
- High catalytic activity during oxygen reduction reaction (ORR)

Conclusions

In this review, the prospect of porosity in nanostructured materials have been summarized particularly for solar and fuel cells. For future photovoltaic research, Porous Si (PSi) can be simultaneously integrated as antireflection coating and Bragg reflector with Si solar cell to improve the overall cell efficiency. Besides, reusability of substrate can highly reduce the cost of solar cell fabrication if Porous Si (PSi) is used as wafer. The use of PSi as substrate for thin film solar cell like Ge, GaAs, GaN requires more focus as it may revolutionize many current research trends which are not limited to solar cell applications. For Dye Sensitized Solar Cell (DSSC), morphology design like Nanorod/Nanosphere, Nanowires/ Nanodonuts along with combination of different materials in heterostructured Photoanode has been seen enhancing the overall cell efficiency of DSSC in some recent research. Considering fuel cells, characteristics of pore in electrodes are controlling factor for better performance and efficient Solid Oxide Fuel Cell (SOFC). Among the three components of SOFC, both electrodes are based on porous materials and emphasis has been given by the researchers mostly for the development of electrodes with controlled porosity in order to enhance the durability of electrodes and lowering the operating temperature of SOFCs.

References

Abud, S.H., Selman, A.M., Hassan, Z., 2016. Investigation of structural and optical properties of GaN on flat and porous silicon. Superlattices and Microstructures 97, 586–590. doi:10.1016/j.spmi.2016.07.017.

Ahmed, B., *et al.*, 2014. Development of novel LSM/GDC composite and electrochemical characterization of LSM/GDC based cathode-supported direct carbon fuel cells. Journal of Solid State Electrochemistry 3, 435–443. doi:10.1007/s10008-013-2284-z.

Aouassa, M., *et al.*, 2012. Ultra-thin planar fully relaxed Ge pseudo-substrate on compliant porous silicon template layer. Applied Physics Letters 101 (23), doi:10.1063/1.4769040.

Aroutiounian, V.M., Martirosyan, K., Soukiassian, P., 2004. Low reflectance of diamond-like carbon/porous silicon double layer antireflection coating for silicon solar cells. Journal of Physics D Applied Physics 25. doi:10.1088/0022-3727/37/19/L01.

Baur, E., Preis, H., 1937. Uber Brennstoff- Ketten Mit Fstleitern. Zeitschrift für Elektrochemie 43, 727–732.

Bertei, A., Nicolella, C., 2011. Percolation theory in SOFC composite electrodes: Effects of porosity and particle size distribution on effective properties. Journal of Power Sources 196 (22), 9429–9436. doi:10.1016/j.jpowsour.2011.06.087.

Bhandaru, S., *et al.*, 2016. Efficiency enhancement via metal-coated porous amorphous silicon back reflectors incorporated in amorphous silicon solar cells. MRS Communications 6 (2), 117–123. doi:10.1557/mrc.2016.15.

Bougoffa, A., *et al.*, 2017. Analytical model of front texturization effect on silicon solar cell with porous silicon at the backside. Optical and Quantum Electronics 49 (1), 1–13. doi:10.1007/s11082-016-0864-8.

Brendel, R., *et al.*, 2003. 15.4%-efficient and 25 ??m-thin crystalline Si solar cell from layer transfer using porous silicon. Physica Status Solidi (A) Applied Research 197 (2), 497–501. doi:10.1002/pssa.200306552.

Calabrese, G., *et al.*, 2014. Ge growth on porous silicon: The effect of buffer porosity on the epilayer crystalline quality. Applied Physics Letters 105 (12), doi:10.1063/1.4894863.

Chang, C.L., *et al.*, 2015. Preparation and characterization of SOFC cathodes made of SSC nanofibers. Journal of Alloys and Compounds 620, 233–239. doi:10.1016/j.jallcom.2014.09.131.

Chaoui, R., Mahmoudi, B., Si Ahmed, Y., 2013. Improvement of screen-printed textured monocrystalline silicon solar cell performance by metal-assisted chemical etching. Energy Procedia 36, 253–259. doi:10.1016/j.egypro.2013.07.029.

Chen, H., *et al.*, 2011. Preparation and characterization of graded SSC – SDC MIEC cathode for low-temperature solid oxide fuel cells. Ceramics International 37 (4), 1209–1214. doi:10.1016/j.ceramint.2010.11.047.

Chen, M., Kim, B.H., Xu, Q., Nam, O.J., Ko, J.H., 2008a. Synthesis and performances of Ni – SDC cermets for IT-SOFC anode. Journal of the European Ceramic Society 28 (15), 2947–2953. doi:10.1016/j.jeurceramsoc.2008.05.009.

Chen, M., Kim, B.H., Xu, Q., Nam, O.J., Ko, J.H., 2008b. Synthesis and performances of Ni-SDC cermets for IT-SOFC anode. Journal of the European Ceramic Society 28 (15), 2947–2953. doi:10.1016/j.jeurceramsoc.2008.05.009.

Chen, M., *et al.*, 2012. Fabrication and electrochemical properties of cathode-supported solid oxide fuel cells via slurry spin coating. Electrochimica Acta 63, 277–286. doi:10.1016/j.electacta.2011.12.115.

Chuangchote, S., Sagawa, T., Yoshikawa, S., 2008. Efficient dye-sensitized solar cells using electrospun TiO_2 nanofibers as a light harvesting layer. Applied Physics Letters 93 (3), 2012–2015. doi:10.1063/1.2958347.

Dees, D., Claar, T., Easler, T., 1987. Conductivity of Porous Ni/ZrO_2-Y_2O_3 Cermets. Journal of the Electrochemical Society 134 (9), 2141–2146.

Ding, L., *et al*., 2017. Promotion on electrochemical performance of a cation deficient SrCo0.7Nb0.1Fe0.2O3−Δ perovskite cathode for intermediate-temperature solid oxide fuel cells. Journal of Power Sources 354, 26–33. doi:10.1016/j.jpowsour.2017.04.009.

Druzhinin, A., *et al*., 2016. Micro- and nanotextured silicon for antireflective coatings of solar cells. Journal of Nano Research 39, 89–95. doi:10.4028/www.scientific.net/JNanoR.39.89.

Duan, Y., *et al*., 2012. Sn-doped TiO_2 photoanode for dye-sensitized solar cells. Journal of Physical Chemistry C 116 (16), 8888–8893. doi:10.1021/jp212517k.

Dzhafarov, T.D., *et al*., 2012. Effect of nanoporous silicon coating on silicon solar cell performance. Vaccum 86 (12), 1875–1879. doi:10.1016/j.vacuum.2012.04.042.

Ferkhi, M., Ahmed, H., 2016. Electrochemical and morphological characterizations of La2−xNiO4±d (x = 0.01, 0.02, 0.03 and 0.05) as new cathodes materials for IT-SOFC. Materials Research Bulletin 83, 268–274. doi:10.1016/j.materresbull.2016.06.009.

Fu, C., *et al*., 2010. Fabrication and evaluation of Ni-GDC composite anode prepared by aqueous-based tape casting method for low-temperature solid oxide fuel cell. International Journal of Hydrogen Energy 35 (1), 301–307. doi:10.1016/j.ijhydene.2009.09.101.

Gao, K., *et al*., 2018. High efficiency multi-crystalline silicon solar cell with inverted pyramid nanostructure High efficiency multi-crystalline silicon solar cell with inverted pyramid nanostructure. Solar Energy 142, 91–96. doi:10.1016/j.solener.2016.12.007.

Gaugain, J.M., 1853. Note sur les signes electriques attribues au mouvement de la chaleur. CR Seances Acad Sciences 37, 82–84.

Ghannam, M.Y., *et al*., 2010. Analysis of thin-film silicon solar cells with plasma textured front surface and multi-layer porous silicon back reflector. Solar Energy Materials and Solar Cells 94 (5), 850–856. doi:10.1016/j.solmat.2010.01.007.

Gouder, S., *et al*., 2014. Investigation of microstructure and morphology for the Ge on porous silicon/Si substrate hetero-structure obtained by molecular beam epitaxy. Thin Solid Films 550, 233–238. doi:10.1016/j.tsf.2013.10.183.

Green, M.A., *et al*., 2015. Solar cell efficiency tables (version 45). Progress in Photovoltaics 23 (1), 1–9. doi:10.1002/pip.

Grove, W.R., 1839. XXIV. On voltaic series and the combination of gases by platinum. Philosophical Magazine Series 3 14 (86), 127–130. doi:10.1080/14786443908649684.

Hafez, H., *et al*., 2010. High efficiency dye-sensitized solar cell based on novel TiO2 nanorod/nanoparticle bilayer electrode. Nanotechnology, Science and Applications 3 (1), 45–51. doi:10.2147/NSA.S11350.

He, B., Ding, D., Xia, C., 2010. Ni – LnO x (Ln = La, Ce, Pr, Nd, Sm, Eu, and Gd) cermet anodes for intermediate-temperature solid oxide fuel cells. Journal of Power Sources 195 (5), 1359–1364. doi:10.1016/j.jpowsour.2009.09.035.

Humphry-Baker, R., *et al*., 2013. Sequential deposition as a route to high-performance perovskite-sensitized solar cells. Nature 499 (7458), 316–319. doi:10.1038/nature12340.

Ivanov, I.I., *et al*., 2013. Porous silicon Bragg mirrors on single- and multi-crystalline silicon for solar cells. Renewable Energy 55, 79–84. doi:10.1016/j.renene.2012.12.031.

Ivers-Tiffee, E., *et al*., 1990. Ceramic and metallic components for a planar SOFC. Berichte der Bunsengesellschaft/Physical Chemistry Chemical Physics 94 (9), 978–981. doi:10.1002/bbpc.19900940919.

Jeong, J., *et al*., 2015. Structural, thermal and electrical conductivity characteristics as anode materials for solid oxide fuel cell. Journal of Solid State Chemistry 226, 154–163. doi:10.1016/j.jssc.2015.02.001.

Jiang, Y., Johnson, C.M., Reece, P.J., *et al*., 2014. Porous silicon omnidirectional bragg reflector for si solar cells. In: Proceedings of the Light, Energy and the Environment, OSA Technical Digest (online), pp. 2–4. Optical Society of America (March 2015). doi:10.1364/PV.2014.PW2B.1.

Kathirvel, S., *et al*., 2016. Solvothermal synthesis of TiO_2 nanorods to enhance photovoltaic performance of dye-sensitized solar cells. Solar Energy 132, 310–320. doi:10.1016/j.solener.2016.03.025.

Kearney, J., Baker, R.T., 2012. Redox and catalytic properties of Ce–Zr mixed oxide nanopowders for fuel cell applications. Catalysis Today 180 (1), 139–147. doi:10.1016/j.cattod.2011.05.018.

Kee, R.J., *et al*., 2008. Solid oxide fuel cells: Operating principles, current challenges, and the role of syngas. Combustion Science and Technology 180 (6), 1207–1244. doi:10.1080/00102200801963458.

Kim, C., *et al*., 2008. Modification of a TiO_2 photoanode by using Cr-doped TiO_2 with an influence on the photovoltaic efficiency of a dye-sensitized solar cell. Journal of Materials Chemistry 18 (47), 5809–5814. doi:10.1039/b805091k.

Kim, M.Y., Lim, D., 2015. The influence of surface texture on the efficiency of crystalline Si solar cells. Journal – Korean Physical Society 67 (6), 1040–1044. doi:10.3938/jkps.67.1040.

Kolchugin, A.A., *et al*., 2016. Structural, electrical and electrochemical properties of calcium-doped lanthanum nickelate. Solid State Ionics. 1–6. doi:10.1016/j.ssi.2016.01.035.

Kong, X., Liu, G., Yi, Z., Ding, X., 2015. $NdBaCu_2O_{5+\delta}$ and $NdBa_{0.5}Sr_{0.5}Cu_2O_{5+\delta}$ layered perovskite oxides as cathode materials for IT-SOFCs, International Journal of Hydrogen Energy 40 (46), 16477-16483, (ISSN 0360-3199), doi:10.1016/j.ijhydene.2015.09.006. http://www.sciencedirect.com/science/article/pii/S0360319915022557).

Kuzma-Filipek, I., *et al*., 2007. Porous silicon as an internal reflector in thin epitaxial solar cells. Physica Status Solidi (A) Applications and Materials Science 204 (5), 1340–1345. doi:10.1002/pssa.200674332.

Kuzma-Filipek, I.J., *et al*., 2008. Chirped porous silicon reflectors for thin-film epitaxial silicon solar cells. Journal of Applied Physics 104 (7), doi:10.1063/1.2993753.

Kwon, H., *et al*., 2011. Investigation of antireflective porous silicon coating for solar cells. ISRN Nanotechnology 2011, 4. doi:10.5402/2011/716409.

Kwon, H., *et al*., 2016. Graphene oxide shells on plasmonic nanostructures lead to high-performance photovoltaics: A model study based on dye-sensitized solar cells. ACS Energy Letters 2 (1), 117–123. doi:10.1021/acsenergylett.6b00612.

Lee, J., *et al*., 2002. Quantitative analysis of microstructure and its related electrical property of SOFC anode, Ni – YSZ cermet. Solid State Ionics 148 (1–2), 15–26.

Li, F., *et al*., 2015. Sponge-like porous TiO_2/ZnO nanodonuts for high efficiency dye-sensitized solar cells. Journal of Power Sources 280, 373–378. doi:10.1016/j.jpowsour.2015.01.118.

Li, Y., *et al*., 2017. Nanoporous palladium anode for direct ethanol solid oxide fuel cells with nanoscale proton-conducting ceramic electrolyte. Journal of Power Sources 340, 98–103. doi:10.1016/j.jpowsour.2016.11.064.

Liu, Y., *et al*., 2013. A stability study of impregnated LSCF-GDC composite cathodes of solid oxide fuel cells. Journal of Alloys and Compounds 578, 37–43. doi:10.1016/j.jallcom.2013.05.021.

Lv, H., *et al*., 2012. Porous-pyramids structured silicon surface with low reflectance over a broad band by electrochemical etching. Applied Surface Science 258 (14), 5451–5454. doi:10.1016/j.apsusc.2012.02.033.

Lv, M., *et al*., 2013. Optimized porous rutile TiO_2 nanorod arrays for enhancing the efficiency of dye-sensitized solar cells. Energy and Environmental Science 6 (6), 1615–1622. doi:10.1039/c3ee24125d.

Mahamdi, R., *et al*., 2018. Ge on porous silicon/Si substrate analyzed by Raman spectroscopy and atomic force microscopy. Journal of Advanced Research in Physics 6 (2), doi:10.13140/RG.2.2.32791.27041.

Mahato, N., *et al*., 2015. Progress in material selection for solid oxide fuel cell technology : A review. Progress in Materials Science 72, 141–337. doi:10.1016/j.pmatsci.2015.01.001.

Mantzouris, X., *et al*., 2008. Physical characterization of Y_2O_3-CeO 2-TiO_2 (YCT) mixed oxides and Ni/YCT cermets as anodes in solid oxide fuel cells. Journal of Materials Science 43 (22), 7057–7065. doi:10.1007/s10853-008-3063-6.

Mao, X., Yu, T., Ma, G., 2015. Performance of cobalt-free double-perovskite $NdBaFe_{2-x}MnxO_{5+\delta}$; cathode materials for proton-conducting IT-SOFC. Journal of Alloys and Compounds 637, 286–290. doi:10.1016/j.jallcom.2015.02.001.

Marrero, N., *et al.*, 2009. Effect of porous silicon stain etched on large area alkaline textured crystalline silicon solar cells. Thin Solid Films 517 (8), 2648–2650. doi:10.1016/j.tsf.2008.09.070.
Mukherjee, K., *et al.*, 2009. Electron transport in electrospun TiO_2 nanofiber dye-sensitized solar cells. Applied Physics Letters 95 (1), 1–4. doi:10.1063/1.3167298.
Nernst, W., 1899. On the electrolytic conductivity of solids at high temperatures. Journal of Electrochemistry 6, 41–43.
Petermann, J.H., *et al.*, 2012. 19%-efficient and 43 μm-thick crystalline Si solar cell from layer transfer using porous silicon. Progress in Photovoltaics: Research and Applications 20 (1), 1–5. doi:10.1002/pip.1129.
Prasad, A., *et al.*, 1982. Porous silicon oxide anti-reflection coating for solar cells. Journal of the Electrochemical Society 129 (3), 596–599. doi:10.1149/1.2123931.
Rabha, M.B., *et al.*, 2011. Combination of silicon nitride and porous silicon induced optoelectronic features enhancement of multicrystalline silicon solar cells. Physica Status Solidi C 8 (6), 1874–1877. doi:10.1002/pssc.201000091.
Rabha, M.B., *et al.*, 2013. Monocrystalline silicon surface passivation by Al_2O_3/porous silicon combined treatment. Materials Science and Engineering B 178 (9), 695–697. doi:10.1016/j.mseb.2012.11.021.
Remache, L., Mahdjoub, A., Fourmond, E., Dupuis, J., Lemiti, M., 2010. Design of porous silicon/PECVD SiO x antireflection coatings for silicon solar cells. In: Proceedings of the International Conference on Renewable Energies and Power Quality (ICREPQ'10), 1 (8), pp. 191–195. doi:10.24084/repqj08.280.
Remache, L., *et al.*, 2016. Optical properties of porous Si/PECVD SiNx:H reflector on single crystalline Si for solar cells. Materials Science- Poland 34 (1), 94–100. doi:10.1515/msp-2016-0054.
Reuter, M., *et al.*, 2009. 50 Mm thin solar cells with 17.0% efficiency. Solar Energy Materials and Solar Cells 93 (6–7), 704–706. doi:10.1016/j.solmat.2008.09.035.
Salman, K.A., Omar, K., Hassan, Z., 2012. Effective conversion efficiency enhancement of solar cell using ZnO/PS antireflection coating layers. Solar Energy 86 (1), 541–547. doi:10.1016/j.solener.2011.10.030.
Savaniu, C.D., Irvine, J.T.S., 2011. La-doped $SrTiO_3$ as anode material for IT-SOFC. Solid State Ionics 192 (1), 491–493. doi:10.1016/j.ssi.2010.02.010.
Search, H., *et al.*, 2006. Almost zero reflectance of a silicon oxynitride/porous silicon double layer antireflection coating for silicon photovoltaic cells. Journal of Physics D Applied Physics 1623, 8–11. doi:10.1088/0022-3727/39/8/022.
Selj, J.H., *et al.*, 2011. Optimization of multilayer porous silicon antireflection coatings for silicon solar cells. Journal of Applied Physics 074904 (2010), 0–10. doi:10.1063/1.3353843.
Shahid Rafique, M., *et al.*, 2018. Material and method selection for efficient solid oxide fuel cell anode: Recent advancements and reviews. International Journal of Energy Research. 1–24. doi:10.1002/er.4210.
Shaikh, S.P.S., Muchtar, A., Somalu, M.R., 2015. A review on the selection of anode materials for solid-oxide fuel cells. Renewable and Sustainable Energy Reviews 51, 1–8. doi:10.1016/j.rser.2015.05.069.
Shi, H., *et al.*, 2012. High performance tubular solid oxide fuel cells with BSCF cathode. International Journal of Hydrogen Energy 37 (17), 13022–13029. doi:10.1016/j.ijhydene.2012.05.061.
Silva, A.R., *et al.*, 2014. The surface texturing of monocrystalline silicon with NH_4OH and ion implantation for applications in solar cells compatible with CMOS technology. Energy Procedia 44 (May 2013), 132–137. doi:10.1016/j.egypro.2013.12.019.
da Silva, F.S., de Souza, T.M., 2017. Novel materials for solid oxide fuel cell technologies: A literature review. International Journal of Hydrogen Energy 42 (41), 26020–26036. doi:10.1016/j.ijhydene.2017.08.105.
Singhal, S., 2000. Advances in solid oxide fuel cell technology. Solid State Ionics 135 (1), 305–313.
Solanki, C.S., *et al.*, 2004. Porous silicon layer transfer processes for solar cells. Solar Energy Materials and Solar Cells 83 (1), 101–113. doi:10.1016/j.solmat.2004.02.016.
Song, M.Y., *et al.*, 2004. Electrospun TiO_2 electrodes for dye-sensitized solar cells. Nanotechnology 15 (12), 1861–1865. doi:10.1088/0957-4484/15/12/030.
Song, X., *et al.*, 2016. Effects of adding alumina to the nickel-zirconia anode materials for solid oxide fuel cells and a two-step sintering method for half-cells. Journal of Power Sources 308, 58–64. doi:10.1016/j.jpowsour.2016.01.070.
Sun, Y., *et al.*, 2016. As a potential solid oxide fuel cell anode material. Journal of Power Sources 301, 237–241. doi:10.1016/j.jpowsour.2015.09.127.
Suzuki, T., Hasan, Z., Yoshihiro Funahashi, T.Y., Yoshinobu Fujishiro, M.A., 2009. Impact of anode microstructure on solid oxide fuel cells. Science 325 (5942), 852–855. doi:10.1126/science.1176404.
Uhlir, A., Uhlir, I., 2005. Historical perspective on the discovery of porous silicon. Physica Status Solidi C: Conferences 2 (9), 3185–3187. doi:10.1002/pssc.200461100.
Wang, J., Bai, D., 2014. Network TiO_2 nanowires for dye-sensitized solar cells. Journal of The Electrochemical Society 161 (5), H265–H268. doi:10.1149/2.005405jes.
Wang, F.Y., Cheng, S., Wan, B.Z., 2008. Porous Ag-CGO cermets as anode materials for IT-SOFC using CO fuel. Fuel Cells Bulletin 2008 (5), 12–16. doi:10.1016/S1464-2859(08)70214-1.
Wang, G., *et al.*, 2013a. Controlled synthesis of mesoporous anatase TiO_2 microspheres as a scattering layer to enhance the photoelectrical conversion efficiency. Journal of Materials Chemistry A 1 (34), 9853. doi:10.1039/c3ta11625e.
Wang, L., *et al.*, 2014. Development of a 16.8% efficient 18-μm silicon solar cell on steel. IEEE Journal of Photovoltaics 4 (6), 1397–1404. doi:10.1109/JPHOTOV.2014.2344769.
Wang, S., *et al.*, 2013b. Fabrication and characterization of a cathode-support solid oxide fuel cell by tape casting and lamination. International Journal of Hydrogen Energy 38 (36), 16584–16589. doi:10.1016/j.ijhydene.2013.08.146.
Wang, W., *et al.*, 2015. Core–shell structured $Li0.33La0.56TiO_3$ perovskite as a highly efficient and sulfur-tolerant anode for solid-oxide fuel cells. Journal of Materials Chemistry A: Materials for Energy and Sustainability 3, 8545–8551. doi:10.1039/C5TA01213A.
Weiying, O., *et al.*, 2011. Optical and electrical properties of porous silicon layer formed on the textured surface by electrochemical etching. Journal of Semiconductors 32 (5), 4. doi:10.1088/1674-4926/32/5/056002.
Wilkins, M.M., *et al.*, 2013. Multijunction solar cell designs using silicon bottom subcell and porous silicon compliant membrane. IEEE Journal of Photovoltaics 3 (3), 1125–1131. doi:10.1109/JPHOTOV.2013.2261931.
Wu, X., *et al.*, 2016. Enhanced electrochemical performance and carbon anti-coking ability of solid oxide fuel cells with silver modified nickel-yttrium stabilized zirconia anode by electroless plating. Journal of Power Sources 301, 143–150. doi:10.1016/j.jpowsour.2015.10.006.
Wu, X., *et al.*, 2018. Preparation of freestanding GaN wafer by hydride vapor phase epitaxy on porous silicon. Superlattices and Microstructures 117, 293–297. doi:10.1016/j.spmi.2018.03.057.
Xia, L.N., *et al.*, 2016. Synthesis and properties of $SmBaCo_2$-$xNixO_{5+\delta}$ perovskite oxide for IT-SOFC cathodes. Ceramics International 42 (1), 1272–1280. doi:10.1016/j.ceramint.2015.09.062.
Xiao, J., *et al.*, 2010. Reflectivity of porous-pyramids structured silicon surface. Applied Surface Science 257 (2), 472–475. doi:10.1016/j.apsusc.2010.07.014.
Yan, K., *et al.*, 2011. A double layered photoanode made of highly crystalline TiO_2 nanooctahedra and agglutinated mesoporous TiO_2 microspheres for high efficiency dye sensitized solar cells. Energy and Environmental Science 4 (6), 2168–2176. doi:10.1039/c1ee01071a.
Yang, M., *et al.*, 2017. TiO_2 nanoparticle/nanofiber-ZnO photoanode for the enhancement of the efficiency of dye-sensitized solar cells. RSC Advances 7 (66), 41738–41744. doi:10.1039/c7ra07644d.
Yang, T., Sezer, H., Celik, I.B., Finklea, H.O., Gerdes, K., 2015. Prediction of SOFC performance with or without experiments: A study on minimum requirements for experimental data. ECS Transactions 68 (1), 2397–2411.
Ye, M., *et al.*, 2013a. Facile and effective synthesis of hierarchical TiO_2 spheres for efficient dye-sensitized solar cells. Nanoscale 5 (14), 6577–6583. doi:10.1039/c3nr01604h.
Ye, M., *et al.*, 2013b. Hierarchically structured nanotubes for highly efficient dye-sensitized solar cells. Advanced Materials 25 (22), 3039–3044. doi:10.1002/adma.201205274.
Zhan, Z., *et al.*, 2011. A reduced temperature solid oxide fuel cell with nanostructured anodes. Energy and Environmental Science 4 (10), 3951–3954. doi:10.1039/c1ee01982a.

Zhan, Z., *et al*., 2013. Mn1.5Co1.5O4−δ infiltrated yttria stabilized zirconia composite cathodes for intermediate-temperature solid oxide fuel cells. International Journal of Hydrogen Energy 38 (36), 16563–16568. doi:10.1016/j.ijhydene.2013.04.106.

Zhang, K., *et al*., 2015. Multifunctional alumina/titania hybrid blocking layer modified nanocrystalline titania films as efficient photoanodes in dye sensitized solar cells. Journal of Power Sources 282, 596–601. doi:10.1016/j.jpowsour.2015.02.092.

Zhao, Y., *et al*., 2017. Sm0.5Ba0.5MnO3-δ anode for solid oxide fuel cells with hydrogen and methanol as fuels. Catalysis Today 298, 33–39. doi:10.1016/j.cattod.2017.06.034.